energies

MDPI

Article

Techno-Economic Optimization of an Off-Grid Solar/Wind/Battery Hybrid System with a Novel Multi-Objective Differential Evolution Algorithm

Yong Yang [1,2] and Rong Li [1,2,*]

[1] School of Energy and Power Engineering, Nanjing Institute of Technology, Nanjing 211167, China; j00000080020@njit.edu.cn
[2] College of Water Conservancy and Hydropower Engineering, Hohai University, Nanjing 210098, China
* Correspondence: njit_lr@njit.edu.cn

Received: 12 March 2020; Accepted: 27 March 2020; Published: 1 April 2020

Abstract: Techno-economic optimization of a standalone solar/wind/battery hybrid system located in Xining, China, is the focus of this paper, and reliable and economic indicators are simultaneously employed to address the problem. To obtain a more precise Pareto set, a novel multi-objective differential evolution algorithm is proposed, where differential evolution with a parameter-adaptive mechanism is applied in the decomposition framework. The algorithm effectiveness is verified by performance comparisons on the benchmark test problems with two reference algorithms: a non-dominated sorting genetic algorithm and a multi-objective evolution algorithm based on decomposition. The applicability of the proposed algorithm for the capacity-optimization problem is also validated by comparisons with the same reference algorithms above, where the true Pareto set of the problem is approximated by combining of the three algorithms through the non-dominant relationship. The results show the proposed algorithm has the lowest inverted generational distance indicator and provides 85% of the true Pareto set. Analyses of the Pareto frontier show that it can produce significant economic benefits by reducing reliability requirements appropriately when loss of power supply probability is less than 0.5%. Furthermore, sensitivity analyses of the initial capital of wind turbine, photovoltaic panel and battery system are performed, and the results show that photovoltaic panel's initial capital has the greatest impact on levelized cost of electricity, while the initial capital of wind turbine has the least impact.

Keywords: hybrid energy system; techno-economic optimization; decomposition; parameter adaptive mechanism; differential evolution

1. Introduction

To address the energy crisis and environmental pollution caused by the growth of the economy and society, hybrid renewable energy systems (HRES) have become popular and wise choices, especially for remote or island areas, where renewable energy is abundant, and where power electricity construction cost is high [1,2]. With their complementary characteristics and matured technologies, HRES consisting of photovoltaics (PV), wind turbines (WT) and battery systems (BS) have become one of the most popular power generation modes [3]. The optimal capacity of HRES is a key and complicated issue [4] because it always contains multiple optimization objectives and is influenced by many factors, such as characteristics of the energy source, technical specifications and environmental conditions [5].

Many researchers have been keen to address the capacity optimization problem. Scholars have applied mathematical programming to solve capacity optimization problems. Linear programming was utilized for capacity optimization of a standalone PV/WT HRES in [6], mixed-integer linear

programming was applied for the design for an isolated PV/WT/BS/DG (diesel generator) HRES in [7] and dynamic programming was utilized for storage capacity optimization of PV/WT/BS HRES in [8]. There are also scholars solving the problem by iteration. An iterative algorithm [9] and an enumeration-based iterative algorithm [10] were implemented for component capacity optimization of micro-grids. However, the methods above have the drawbacks that they can only handle single objective optimization and are susceptible to falling into local optimum solutions [11].

Many other researchers utilized software tools to solve this problem. HOMER [12,13] is one of the most popular tools. It was used for capacity optimization, techno-economic and sensitivity analyses of a PV/BS HRES in [14] and a PV/DG/BS HRES in [15]. In [16], the techno-economic feasibility of replacing a completely DG power supply by a standalone PV/WT/BS/DG was analyzed by HOMER. In [17], the performance of a WT/BS/DG HRES impacted by different battery technologies was analyzed by HOMER. It was applied for the investigation of possible renewable power generation systems for Gadeokdo Island in South Korea in [18]. In [19], component capacities of PV/BS/DG HRES was optimized under different load profiles. In [20], the optimal sizing of fuel cell/PV HRES was performed by HOMER with the components cost calculated by fuzzy logic program. Homer is good software for scenario investigation, but some scenarios need to be re-calculated individually for the specific situation because this tool can only handle single-object optimization [21], the flexibility is limited, and is easy to fall into local optimum solutions [22].

Intelligent optimization algorithms, having the superiority of global optimization and the capacity to handle multi-objective problems easily, have been intensively studied in the optimal capacity problem [11]. In [23], an artificial bee colony algorithm was used for finding the optimal capacities of a PV-biomass HRES with the minimum levelized cost of electricity (LCOE), and the results proved it outperformed HOMER. The discrete bat search algorithm [24] and grasshopper optimization algorithm [25] were used for PV/WT/DS/BS HRES. Many researchers have considered multiple objective functions in capacity optimization, and have applied multi-objective intelligent optimization algorithms to obtain solutions. In [26], a multi-objective differential evolution algorithm was applied for the capacity optimization of a PV/WT/DG/BS HRES in Yanbu, where the objective functions were minimizing LCOE and loss of power supply probability (LPSP) simultaneously. A non-dominated sorting genetic algorithm (NSGA-II) was applied for optimal sizing of an off-grid PV/WT/BS HRES where economic and reliability indicators were simultaneously considered in [27]. Many scholars considered additional indicators, except for economic and reliability indicators; for example, an environmental indicator was involved in the optimal sizing of a PV/WT/fuel cell HRES in [28] and a PV/WT/BS HRES in [29].

With the rapid development of HRES, intelligent optimization algorithms with better performance are urgently needed [11]. Multi-objective evolution algorithms based on decomposition (MOEA/D) [30] provide a new approach to multi-objective optimization [31] and have received growing attention as they can incorporate the techniques used in single-objective optimization algorithms well. In this paper, a novel multi-objective optimization algorithm, namely MOEA/DADE, is proposed for better optimization performance. In this algorithm, a differential evolution mechanism with parameter self-adaptation is integrated in decomposition framework and its effectiveness is verified by algorithm contrasts with NSGA-II and MOEA/D on benchmark problems. Then, the algorithm is applied for techno-economic optimization of a standalone PV/WT/BS HRES located in Xining, China and its applicability for this problem is also validated by comparisons with NSGA-II and MOEA/D. Lastly, techno-economic and sensitivity analyses of the initial capital of wind turbines, photovoltaics and battery systems are performed.

The paper is organized as follows: component models of the HRES and energy management strategy (EMS) are introduced in Section 2, MOEA/DADE algorithm and algorithm comparisons with MOEA/D and NSGA-II on benchmark problems are presented in Section 3, techno-economic optimization and sensitivity analyses of PV/WT/BS HRES are performed in Section 4; finally, conclusions are drawn in Section 5.

2. Component Models and Energy Management Strategy

The HRES is consisted of five major components: PV systems, WT systems, a converter, BS and grid loads. Its structure diagram is shown in Figure 1.

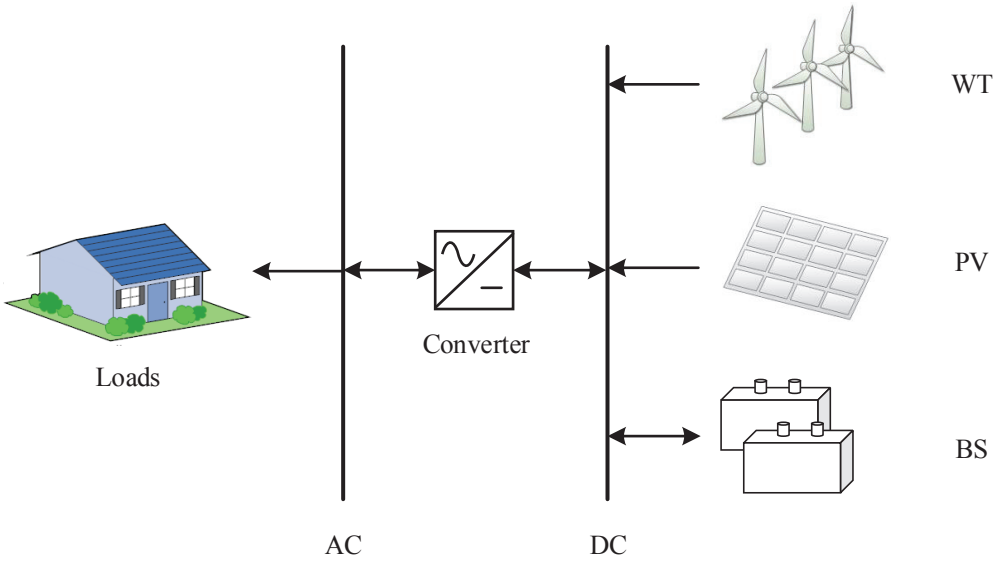

Figure 1. Structure diagram of photovoltaic/wind turbine/battery system hybrid renewable energy system (PV/WT/BS HRES).

2.1. Wind turbine

The relationship between a WT's output power (P_{WT}) and wind speed can be described by a piecewise function as Equation (1) [13]:

$$P_{WT}(t) = \begin{cases} 0 & v \le v_{cut-in} \text{ or } v \ge v_{cut-out} \\ P_r\left(\frac{v^3 - v_{cut-in}^3}{v_r^3 - v_{cut-in}^3}\right) & v_{cut-in} \le v \le v_r \\ P_r & v_r \le v \le v_{cut-out} \end{cases} \quad (1)$$

where P_r (kW) represents the WT's rated output power, v (m/s) represents wind speed at the turbine hub height, v_{cut-in} (m/s) is the cut-in speed, v_r (m/s) is the rated speed, and $v_{cut-out}$ (m/s) is the cut-out speed. v_{cut-in}, v_r and $v_{cut-out}$ are assumed to be 2 (m/s), 9 (m/s) and 24 (m/s) respectively.

As the anemometer is not at the same altitude as the turbine hub, v can be obtained by Equation (2):

$$v = v_{ref} \times \left(\frac{h}{h_{ref}}\right)^{\gamma} \quad (2)$$

where h(m), h_{ref} (m) are the installation altitude of the turbine hub and the anemometer respectively, v_{ref} (m/s) is the wind speed measured by anemometer, γ is a constant number between 0.1 and 0.25 [13]. In this paper, the anemometer height is 10 m, the hub height is 25 m and γ is assumed 0.25.

2.2. PV Panel

Ignoring the temperature effects, the PV's output power (P_{PV}) can be calculated by Equation (3) [13],

$$P_{PV}(t) = Y_{PV} f_{PV}\left(\frac{G_t}{G_{STC}}\right) \quad (3)$$

where Y_{PV} (kW) and G_{STC} (1 kW/m^2) represent the power output and solar radiation under standard test conditions, G_t (kW/m^2) represents the actual solar incident radiation on the PV array in time t, and f_{PV}(%) is the PV derating factor.

2.3. Battery System

The electric power stored into the BS in time t is described as Equation (4):

$$P_B(t) = P_{WT}(t) + P_{PV}(t) - P_L(t)/\eta_{inv} \tag{4}$$

where P_L (kW) represents the electrical load, η_{inv} represents the converter efficiency.

If $P_B(t)$ is greater than 0, the BS will be charged to store the surplus power energy, otherwise, it will be discharged to make up for the electricity shortage. The BS's state of charge (SOC) for t period is shown as Equation (5):

$$SOC_B(t) = (1-\sigma) \cdot SOC_B(t-1) + \alpha(t) P_B(t) \Delta t \tag{5}$$

where SOC_B (kW·h) is the BS's SOC, t represents time index, and σ is the dissipation coefficient. Assume that the charge efficiency (η_c) and discharge efficiency (η_d) remain unchanged, $\alpha(t)$ can be obtained by Equation (6).

$$\alpha(t) = \begin{cases} \eta_c & P_B(t) > 0 \\ \frac{1}{\eta_d} & P_B(t) < 0 \end{cases} \tag{6}$$

Moreover, the BS's SOC should satisfy the constraint described as Equation (7):

$$(1 - DOD) \cdot E_{bmax} \le SOC(t) \le E_{bmax} \tag{7}$$

where E_{bmax} (kW·h) means the maximum allowable amounts of energy that can be stored by the BS, DOD (%) is the BS's allowable depth of discharge.

2.4. Load Profile

To make the inherently statistical power load more realistic, the load in each time step is obtained by multiplying its annual average value with a perturbation factor k_{cv} [32] shown as Equation (8):

$$k_{cv} = 1 + \alpha_d + \alpha_t \tag{8}$$

where $\alpha_d \sim N(0, \delta_d^2)$ denotes the daily variation percent, $\alpha_t \sim N(0, \delta_t^2)$ denotes the hourly variation percent.

2.5. Economic Model

The life cycle cost (LCC) of the k-th component of the HRES is described as Equation (9). It includes initial capital cost (IC_k), maintenance and operation cost ($O\&M_k$), replacement cost (Rp_k) and salvage value (RV_k).

$$LCC_k = IC_k + O\&M_k + Rp_k - RV_k \tag{9}$$

IC_k, $O\&M_k$, Rp_k, RV_k can be calculated according to Equations (10)–(15), where C_k (kW for WT, PV and converter, and kW·h for BS) means the component capacity, γ_k, θ_k and π_k mean initial capital cost, maintenance and operation cost, replacement cost per unit respectively and their units are \$/kW for WT, PV and converter and \$/kW·h for BS, N (year) and N_k (year) mean the system life time of the system and the k-th component respectively, N_k^{rem} (year) means the surplus life of the k-th component when the system ends, R_k^{rp} (year) means the last replaced time of the k-th component, INT(.) is a function that returns the smallest integer that is greater than or equal to the input number, and the

relationship of the real discount rate i_r (%), nominal discount rate r (%) and expected inflation rate u (%) is shown as Equation (16):

$$IC_k = \gamma_k C_k \tag{10}$$

$$O\&M_k = \theta_k C_k \sum_{j=1}^{N} (\frac{1}{1+i_r})^j \tag{11}$$

$$Rp_k = \pi_k C_k \sum_{m=1}^{\mathrm{INT}[\frac{N}{N_k}]-1} (\frac{1}{1+i_r})^{m \times N_k} \tag{12}$$

$$RV_k = \pi_k C_k \frac{N_k^{\mathrm{rem}}}{N_k} (\frac{1}{1+i_r})^N \tag{13}$$

$$N_k^{\mathrm{rem}} = N_k - (N - R_k^{\mathrm{rp}}) \tag{14}$$

$$R_k^{\mathrm{rp}} = N_k \cdot \mathrm{INT}(\frac{N}{N_k}) \tag{15}$$

$$i_r = \frac{r-u}{r+u} \tag{16}$$

Capital recovery factor (CRF) shown as Equation (17) is applied to convert LCC into the annualized cost of the HRES. Assuming that the amount of electricity generated by the HRES per year stays the same over the project's lifetime, LCOE is shown as Equation (18) [24]:

$$\mathrm{CRF}(i_r, N) = \frac{i_r(1+i_r)^N}{(1+i_r)^N - 1} \tag{17}$$

$$\mathrm{LCOE} = \mathrm{CRF}(i_r, N) \cdot \frac{\sum_{k=1}^{NC} LCC_k}{E_{\mathrm{load}}} \tag{18}$$

where NC is the number of components in the HRES and E_{load} (kW·h) is the annual power output.

2.6. Rule-Based Energy Management Strategy

EMS is one main criterion for HRES [25]. To coordinate various components' output power, a rule-based EMS is designed and its flow chart is shown as Figure 2.

Firstly, a binary variable (S_p) is defined to represent whether the electric power generated is sufficient, and a binary variable (S_c) is defined to represent whether the converter capacity is sufficient. Their definitions are shown as Equations (19) and (20).

$$S_p = P_{PV}(t) + P_{WT}(t) - P_L(t)/\eta_{inv} \tag{19}$$

$$S_c = C_{inv} - P_L(t)/\eta_{inv} \tag{20}$$

Secondly, according to the combination values of S_p and S_c, the rule-based EMS is designed with four case scenarios as follows: Case 1,the electric power generated and the converter capacity are both sufficient ($S_p > 0$ and $S_c > 0$); Case 2, the electric power generated is sufficient while the converter capacity is insufficient ($S_p > 0$ and $S_c < 0$); Case 3, the electric power generated is insufficient while the converter capacity is sufficient ($S_p < 0$ and $S_c > 0$); and, Case 4, the electric power generated and the converter capacity are both insufficient ($S_p < 0$ and $S_c < 0$).

Finally, update the BS's SOC and calculate the loss of power supply (LPS) for different cases according to the follow rules:

Case 1: the load will be completely satisfied (LPS = 0), and the extra power used for charging the battery is calculated by Equation (4) and a new temporary SOC of the BS (*soc_new*) can be obtained by

Equation (5), if $soc_new < E_{\mathrm{bmax}}$, set $soc(t+1) = soc_new$, otherwise, set $soc(t+1) = E_{\mathrm{bmax}}$ and the extra energy will be discarded.

Case 2: the power output of the HRES will be $\eta_{\mathrm{inv}} \cdot C_{\mathrm{inv}}$, LPS and the power used for charging the BS (P_{B}) can be calculated by Equations (21) and (22) respectively.

$$LPS(t) = P_{\mathrm{L}}(t) - C_{\mathrm{inv}} \cdot \eta_{\mathrm{inv}} \tag{21}$$

$$P_{\mathrm{B}}(t) = P_{\mathrm{PV}}(t) + P_{\mathrm{WT}}(t) - C_{\mathrm{inv}} \tag{22}$$

then, update the BS's SOC as Case 1.

Case 3: the battery will be discharged to supply as much electricity as possible and whether the load can be satisfied with the BS's support is calculated according to Equation (23).

$$S_{\mathrm{bp}} = P_{\mathrm{PV}}(t) + P_{\mathrm{WT}}(t) + soc(t) - E_{\mathrm{bmin}} - P_{\mathrm{L}} \tag{23}$$

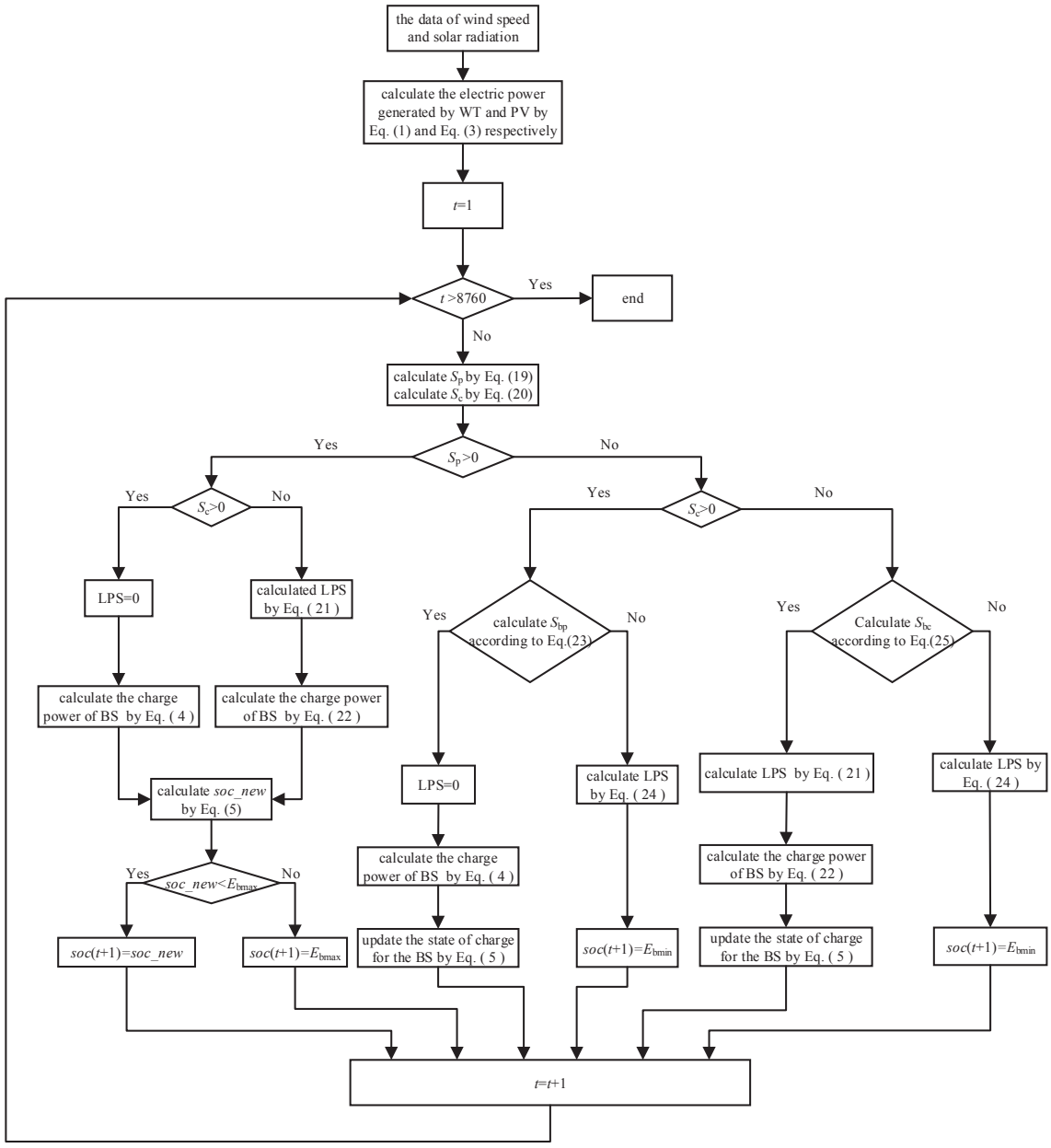

Figure 2. The flow chart of the energy management strategy (EMS).

If $S_{bc} > 0$, the load will be completely satisfied (LPS = 0), and the charge power of BS (P_B) and BS's SOC are calculated by Equations (4) and (5) respectively, otherwise, set $soc(t+1) = E_{bmin}$ and calculate LPS by Equation (24).

$$LPS(t) = P_L(t) - (P_{PV}(t) + P_{WT}(t) + soc(t) - E_{bmin}) \cdot \eta_{inv} \tag{24}$$

Case 4: the load will not be completely satisfied and the battery will be discharged. Firstly, whether the power output can reach to converter capacity with the BS's support is calculated according to Equation (25).

$$S_{bc} = P_{PV}(t) + P_{WT}(t) + soc(t) - E_{bmin} - C_{inv} \tag{25}$$

If $S_{bc} > 0$, the power output of the HRES will be $\eta_{inv} \cdot C_{inv}$, LPS is calculated by Equation (21), the charge power of BS (P_B) and BS's SOC can be calculated by Equation (22) and Equation (5) respectively, otherwise, set $soc(t+1) = E_{bmin}$ and calculate LPS by Equation (24).

2.7. Objective Function and Constraints

The objective functions described as Equation (26) are to maximize system reliability (represented by minimizing LPSP) and economy (represented by minimizing LCOE) simultaneously,

$$\begin{aligned} f = \min\{&\mathrm{LCOE}(C_{pv}, C_{wt}, E_b, C_{inv}), \\ &\mathrm{LPSP}(C_{pv}, C_{wt}, E_b, C_{inv})\} \\ 0 \le C_{pv} \le C_{pv}^{max} \\ 0 \le C_{wt} \le C_{wt}^{max} \\ 0 \le E_b \le E_b^{max} \\ 0 \le C_{inv} \le C_{inv}^{max} \end{aligned} \tag{26}$$

where C_{pv}, C_{wt}, C_{inv}, and E_b are decision variables that mean the capacity of PV, WT, converter and BS respectively, C_{pv}^{max}, C_{inv}^{max} and E_b^{max} are their upper bounds, and LPSP is calculated as Equation (27),

$$\mathrm{LPSP} = \frac{\sum_{t=1}^{T} LPS(t)}{\sum_{t=1}^{T} P_L(t)} \tag{27}$$

where t is a time period index, T (8760 h) represents the total hours of a year.

3. Optimization Algorithm

3.1. MOEA/DADE

MOEA/D whose detailed information can be found in [30] provides a new approach for multi-objective optimization. It has an advantage in that it can incorporate the techniques in single-objective optimization algorithms well, while its performance is greatly impacted by the new solution generation mechanism. For better optimization performance, an adaptive differential evolution mechanism is implemented in MOEA/D and a new algorithm, namely MOEA/DADE, is proposed in this paper.

3.1.1. Differential Evolution Mechanism

The differential evolution mechanism is applied for new individual's generation as Equation (28),

$$y_k = \begin{cases} x_i(t) + F_i \cdot (x_{r_1}(t) - x_{r_2}(t)) & \text{rand} \le Cr_i \text{ or } j = k \\ x_{i,j}(t) & \text{otherwise} \end{cases} \tag{28}$$

where F_i and Cr_i, in the range of [0,1], represent the scale factor and crossover rate respectively, r_1 and r_2 are randomly selected from set P. The definition of P is shown as Equation (29),

$$P = \begin{cases} B_i & \text{if rand}<\delta \\ \{1, \ldots, N\} & \text{otherwise} \end{cases} \tag{29}$$

where B_i represents the neighbor set of the individual i and $\{1, \ldots, N\}$ represents the collection of the all individuals, and $\delta \in (0, 1)$. Equation (29) means the individuals used for differential information generation can be selected from the whole individuals according to a tiny probability $(1 - \delta)$ and this is helpful for maintaining individual diversity.

3.1.2. Parameter Adaptive Mechanism

In differential evolution mechanism, the control parameters (F_i and Cr_i) have great impact on the quality of new individuals, and their values should be different for different stages of the evolution process. Thus, a parameter adaptive mechanism is applied to the algorithm [33].

Firstly, at each generation, the control parameters (F_i and Cr_i) of each individual are independently generated according to Equations (30) and (31), respectively,

$$Cr_i = \text{randn}_i(\mu_{\text{Cr}}, 0.1) \tag{30}$$

$$F_i = \text{randc}_i(\mu_{\text{F}}, 0.1) \tag{31}$$

where $\text{randn}_i(\mu_{\text{Cr}}, 0.1)$ means a standard normal distribution with mean and variance of μ_{Cr} and 0.1, $\text{randc}_i(\mu_{\text{F}}, 0.1)$ means a Cauchy distribution with mean and variance of μ_{F} and 0.1. The control parameters will be reinitialized until they are in range of [0,1].

Secondly, record the control parameters that generate better individuals by set S_{Cr} and S_{F}.

Lastly, update μ_{Cr} and μ_{F} at the end of each generation according to Equations (32) and (33),

$$\mu_{\text{Cr}} = (1 - c) \cdot \mu_{\text{Cr}} + c \cdot \text{mean}_{\text{A}}(S_{\text{Cr}}) \tag{32}$$

$$\mu_{\text{F}} = (1 - c) \cdot \mu_{\text{F}} + c \cdot \text{mean}_{\text{L}}(S_{\text{F}}) \tag{33}$$

where c is a weighting factor, $\text{mean}_{\text{A}}(S_{\text{Cr}})$ means the average value of the elements in set S_{Cr} and $\text{mean}_{\text{L}}(S_{\text{F}})$ is calculated by Equation (34).

$$\text{mean}_{\text{L}}(S_{\text{F}}) = \frac{\sum_{F \in S_{\text{F}}} F^2}{\sum_{F \in S_{\text{F}}} F} \tag{34}$$

3.2. Algorithm Contrast

To verify the effectiveness of MOEA/DADE, algorithm contrasts with MOEA/D and NSGA-II are performed on PlatEMO v2.1 [34]. In the contrast test, the benchmark problems are ZDT1~ZDT4 and ZDT6 as proposed in [35], their dimensions (D) are 30 and objective function numbers are 2. Parameters for each algorithm are represented as Table 1, the maximum evaluation number for each algorithm are 10,000 and all three algorithms run 30 times. A comprehensive indicator IGD [36] defined as Equation (35), which can reflect both the diversity and convergency of the Pareto set (PS), is chosen to evaluate the algorithm performance.

$$\text{IGD}(P^*, P) = \frac{\sum_{x^* \in P^*} \min_{x \in P} \text{d}(x^*, x)}{|P^*|} \tag{35}$$

where P^* represents sampling points from the true Pareto frontier (PF), P represents the PF obtained by the optimization algorithm, $\text{d}(x^*, x)$ represents the Euler distance between any two elements in P^* and P, and $|P^*|$ denotes the number of elements of P^*.

Table 1. Parameters of NSGA-II, MOEA/D and MOEA/DADE.

Algorithm	Parameters
NSGA-II	$P_c = 0.9$, $P_m = 1/D$, $\eta_c = 20$, $\eta_m = 20$
MOEA/D	$T = 10$, $P_c = 0.9$, $P_m = 1/D$, $\eta_c = 20$, $\eta_m = 20$
MOEA/DADE	$T = 10$, $\mu_{Cr} = 0.8$, $\mu_F = 0.5$, $\delta = 0.9$

The test results are presented in Table 2. From the table, we can see that MOEA/DADE outperforms MOEA/DADE and NSGA-II on all the functions except for ZDT4. It indicates MOEA/DADE is a cost-effective multi-objective optimization algorithm for most of the considered test problems, but not for all considered functions. This behavior is not an exception but actually verifies the statement of No Free Lunch theorem. The reasons for superior performance may be concluded as two aspects: (1) the algorithm is implemented in the decomposition framework where evolution is achieved through the cooperation of neighboring individuals, and this mechanism is different from NSGA-II; (2) a differential evolution mechanism with parameter self-adaptation is applied whose effectiveness has been demonstrated in single-objective optimization.

Table 2. Test results of NSGA-II, MOEA/D and MOEA/DADE with D = 30 for each function.

Function	NSGA-II Mean (std)	MOEA/D Mean (std)	MOEA/DADE Mean (std)
ZDT1	1.7218×10^{-1} (1.10×10^{-1}) –	1.6737×10^{-1} (5.91×10^{-2}) –	4.7928×10^{-2} (1.62×10^{-2})
ZDT 2	5.5298×10^{-1} (1.01×10^{-1}) –	3.2507×10^{-1} (1.88×10^{-1}) –	1.2261×10^{-1} (1.63×10^{-1})
ZDT 3	1.3700×10^{-1} (8.06×10^{-2}) –	2.1748×10^{-1} (1.12×10^{-1}) –	6.6407×10^{-2} (3.45×10^{-2})
ZDT 4	1.4230×10^{1} (4.08×10^{0}) +	1.4189×10^{1} (4.79×10^{0}) +	3.8489×10^{1} (9.88×10^{0})
ZDT 6	3.8877×10^{0} (3.78×10^{-1}) –	2.3380×10^{0} (4.81×10^{-1}) –	1.8724×10^{0} (3.83×10^{-1})
+/-/=	1/4/0	1/4/0	

4. Case Study

4.1. Data

The HRES studied in this paper is located in Xining (47°29′ N, 104°17′ E), China. Its nameplate life is 25 years. The technical and economical parameters are presented as Table 3 [37]. A year's data of solar radiation and wind speed were obtained from HOMER Pro [13] and their annual average values are 4.67 (kW·h/m^2/day) and 6.63 (m/s) respectively. The load profile is obtained by Equation (8) where δ_d and δ_t are assumed 10% and 20% respectively. The data profile of load, solar radiation and wind speed of each hour are shown as Figure 3.

Table 3. Technical and economical parameters of the HRES.

	Factor	Value		Factor	Value
Project	Lifetime (year)	25	Battery	Lifetime (year)	10
	Discount rate (%)	6		Initial capital ($/kW·h)	160
	Inflation rate (%)	2		Replacement ($/kW·h)	128
PV	Lifetime (year)	25		O&M ($/year/kW·h)	1
	Initial capital ($/kW)	1857		Round trip efficiency (%)	80
	Replacement ($/kW)	1486	Converter	Lifetime (year)	15
	O&M ($/year/kW)	18		Initial capital ($/kW)	890
Wind Turbine	Lifetime (year)	20		Replacement ($/kW)	800
	Initial capital ($/kW)	1610		O&M ($/year/kW)	10
	Replacement ($/kW)	1288		Efficiency (%)	95
	O&M ($/year/kW)	32			

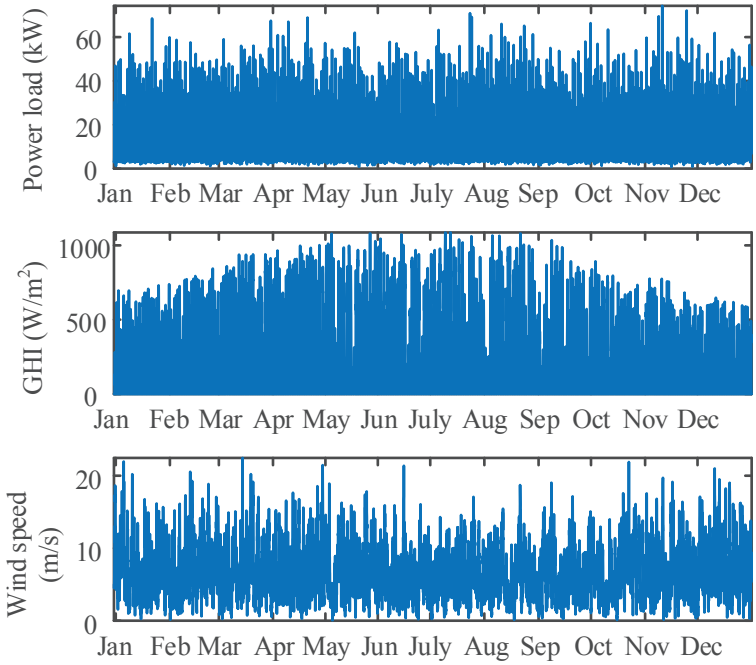

Figure 3. The data profile of load, solar radiation and wind speed for each hour.

4.2. Techno-Economic Analysis

To validate the applicability of MOEA/DADE for the capacity optimization problem, comparisons with MOEA/D and NSGA-II were performed. The processes of evaluating individuals of MOEA/DADE, MOEA/D and NSGA-IIare the same and are shown in Figure 4.

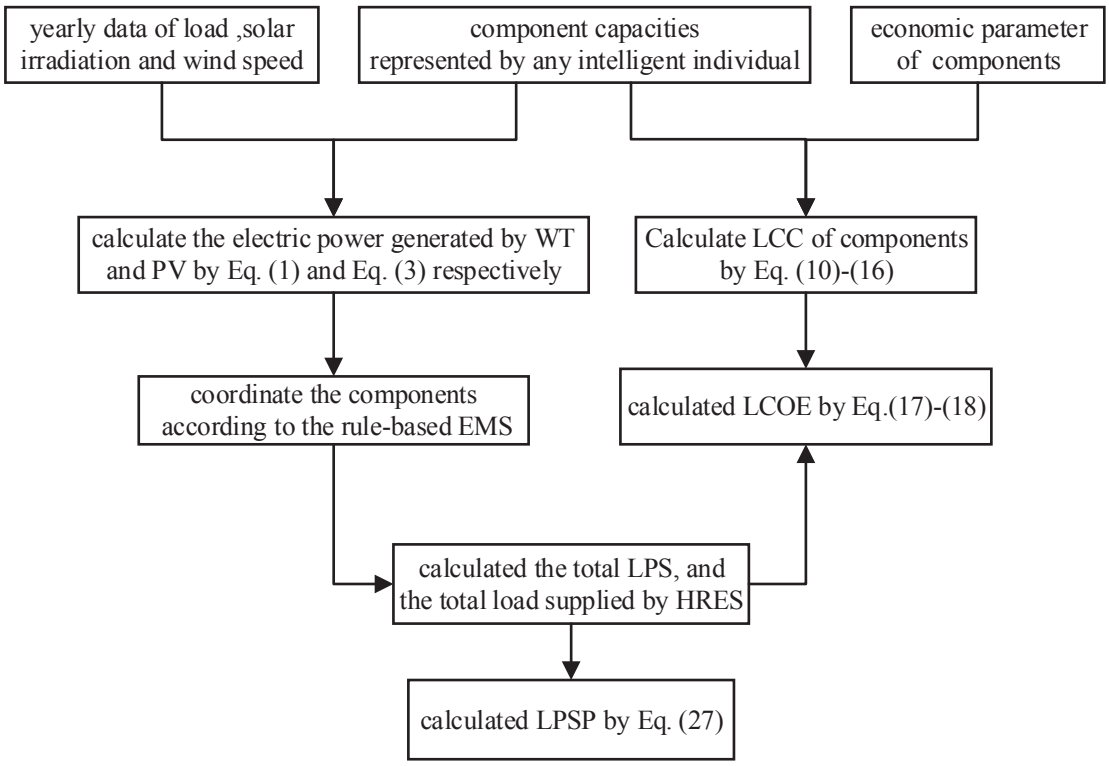

Figure 4. The process of evaluating individuals of MOEA/DADE, MOEA/D and NSGA-II.

The decision variables' ranges are presented as $C_{pv} \in [0\ 500]$, $C_{inv} \in [0, 500]$, $E_b \in [0, 3600]$. For this problem, its true PS and PF are unknown. To evaluate algorithm performance, a method combining of MOEA/DADE, MOEA/D and NSGA-IIis proposed to approximate the true PS and PF. Firstly, all the three algorithms are run 20 times respectively to obtain their corresponding PSs; secondly, a temporary set is created by merging all the PSs; finally, the true PS and PF are obtained from the temporary set according to the non-dominant relationship.

The PFs obtained by each algorithm and the approximate true PF are represented as Figure 5. From it, we can see the PF obtained by MOEA/DADE almost coincides with the approximate true PF. There are 81 groups of unduplicated solutions in the approximately true PS, among them MOEA/DADE provides 67 groups (82.72%), NSGA-II provides 13 groups (16.05%) and MOEA/D provides 1 group (1.23%).

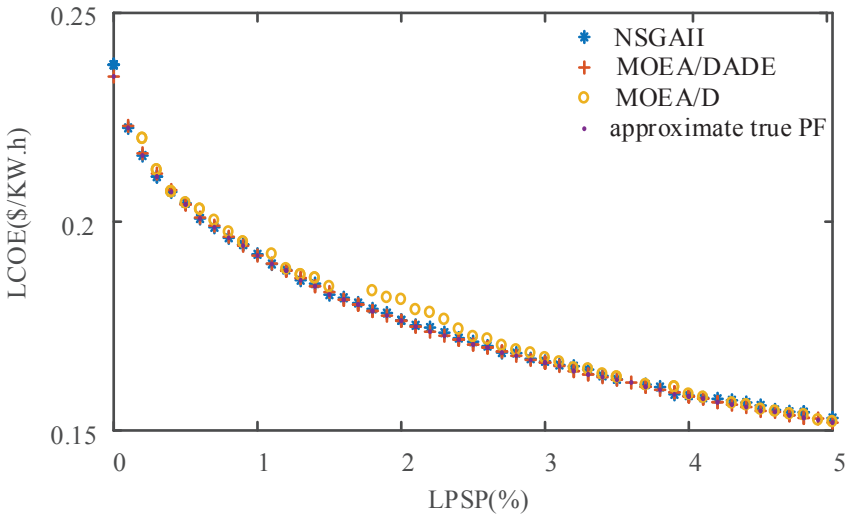

Figure 5. The Pareto frontier (PF) of NSGA-II, MOEA/D, MOEA/DADE and the approximation.

IGD indicators calculated based on the approximate true PS are shown as Table 4. From it, we can see MOEA/DADE has the minimal IGD. From analysis of Figure 5 and Table 4, it can be concluded that MOEA/DADE is more suitable for this capacity optimization problem than NSGA-II and MOEA/D.

Table 4. IGD indicators for NSGA-II, MOEA/D and MOEA/DADE.

Algorithm	NSGA-II	MOEA/D	MOEA/DADE
IGD	4.7809×10^{-4}	1.3926×10^{-3}	7.5655×10^{-5}

To analyze the relationship of the reliability (LPSP) and economy (LCOE), the slope of LCOE is calculated according to Equation (36).

$$slope = \frac{\Delta LCOE}{\Delta LPSP} \tag{36}$$

The slope of LCOE varying with LPSP is presented as Figure 6. From it, we can see LCOE and LPSP are negatively related, and the absolute value of the slope decreases gradually with the increase of LPSP when LPSP is less than 2%, and almost stays at a small value when LPSP is in the range of 2% to 5%. The absolute value of the slope decreases rapidly and falls from 0.1231 ($/kW·h) to 0.0033 ($/kW·h) when LPSP is less than 0.5%, slows down and stays in the range of [0.0110,0.0335] ($/kW·h) when LPSP is in the range of [0.5%,2%], and is almost unchanged when LPSP is larger than 2% with a small average value 0.0081 ($/kW·h). From Figure 6, it can be concluded that the economic benefits are significant by reducing reliability requirements when LPSP is less than 0.5%, and not obvious when LPSP is larger than 0.5%. For example, the system's LCOE can fall from 0.2348 ($/kW·h) to 0.2225

($/kW·h), falling by 0.0123 ($/kW·h) as LPSP increases by 0.1% when LPSP is 0; however, it can only fall from 0.2041 ($/kW·h) to 0.2008 ($/kW·h), falling by 0.0033 ($/kW·h) as LPSP increases by 0.1% when LPSP is 0.5%.

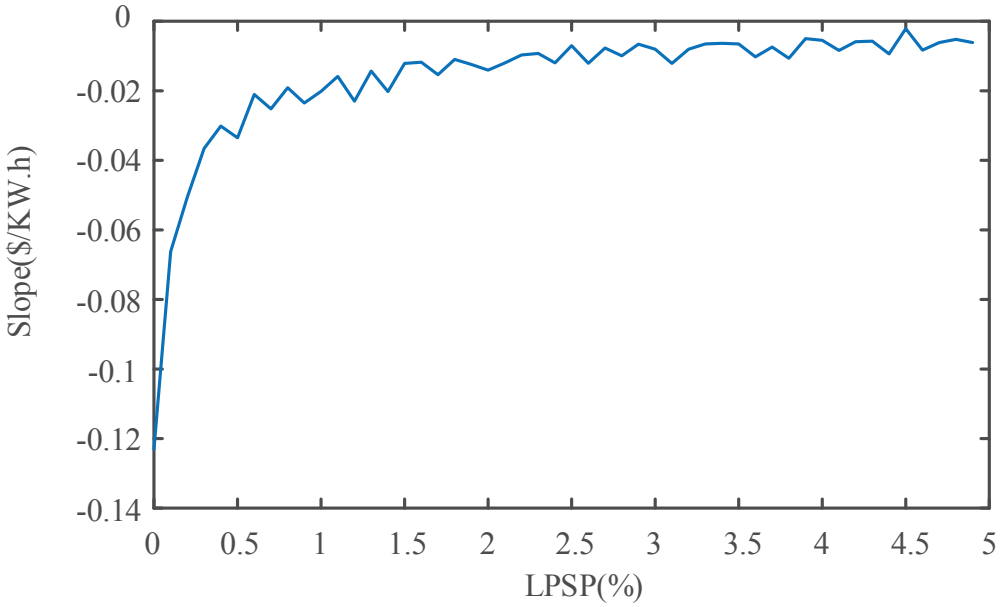

Figure 6. The slope of minimum levelized cost of electricity (LCOE) varying with loss of power supply probability (LPSP).

4.3. Sensitivity Analysis

Sensitivity analysis was performed to investigate the impact of initial capital of WT, PV and BS on the LCOE. The sensitivity analysis for any component is carried out by the following steps: (1) let its initial capital be 80%, 90%, 110% and 120% of its initial value respectively while keeping the other parameters unchanged; (2) solve the capacity optimization problem of the HRES by MOEA/DADE; (3) choose the solution with LPSP equal to 0.5% from Pareto set. The effects of components' initial capital on LCOE when LPSP is 0.5% are presented as Figure 7. In Figure 7, the influence on LCOE can be reflected by the slope of the fold line, and the higher slope means a greater impact. From Figure 7, we can see that the PV's line slope is higher than the others, while WT's is lower than the others—that is to say, PV's initial capital has the greatest effect while WT's initial capital has the least effect on LCOE. When the initial capital of PV, BS and WT falls to 80% of its initial value, the LCOE with LPSP equals to 0.5% falls from 0.2348 ($/kW·h) to 0.2255 ($/kW·h) for the PV case (falling by 3.97%), to 0.2297 ($/kW·h) for the BS case (falling by 2.19%) and to 0.2299 ($/kW·h) for the WT case (falling by 2.07%). When components' initial capital increases to 120% of its initial value, the LCOE can reach to 0.2490 ($/kW·h) for the PV case (increasing by 6.05%), to 0.2460 ($/kW·h) for the BS case (increasing by 4.77%) and to 0.2407 ($/kW·h) for the WT case (increasing by 2.50%).

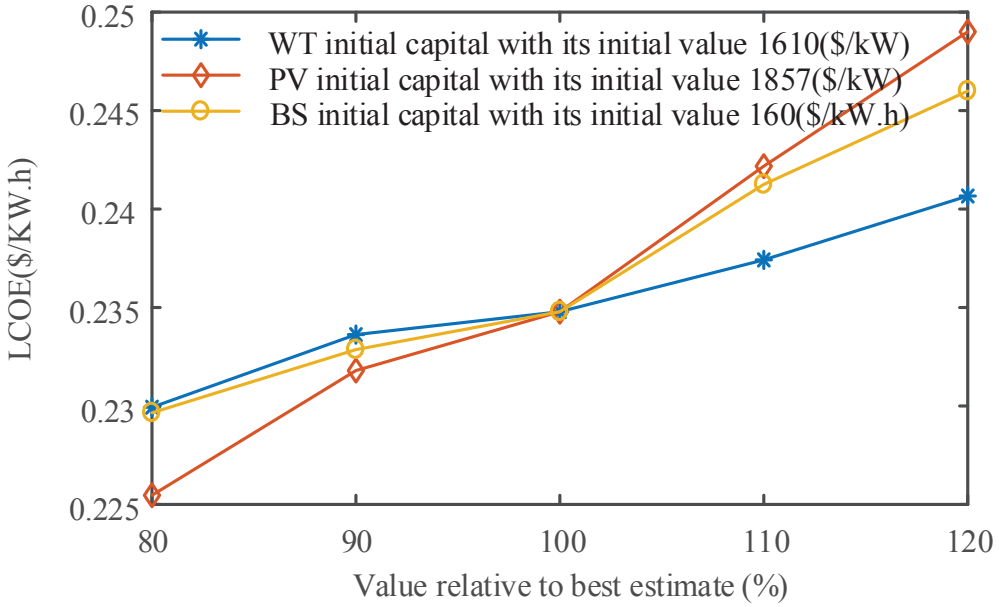

Figure 7. The effects of components' initial capital on LCOE.

5. Conclusions

In this paper, we focused on the techno-economic optimization of a standalone PV/WT/BS HRES in Xining, China. To find out the optimal LCOE under different LPSP, a novel multi-objective optimization algorithm, namely MOEA/DADE, is proposed. In this algorithm, a differential evolution mechanism with parameter self-adaptation is implemented in the decomposition framework. Algorithm comparisons with NSGA-II and MOEA/D on benchmark problems verify that MOEA/DADE is superior to NSGA-II and MOEA/D. The applicability of MOEA/DADE on the capacity optimization problem was also validated by comparisons. Then, MOEA/DADE was applied for techno-economic and sensitivity analyses of the HRES. Techno-economic analyses from the PF shows the economic benefits are significant by reducing reliability requirements when LPSP is less than 0.5%, and are not obvious when LPSP is larger than 0.5%. The system's LCOE can fall from 0.2348 ($/kW·h) to 0.2225 ($/kW·h), falling by 0.0123 ($/kW·h) as LPSP increases by 0.1% when LPSP is 0, however, it can only fall from 0.2041 ($/kW·h) to 0.2008 ($/kW·h), falling by 0.0033 ($/kW·h) as LPSP increases by 0.1% when LPSP is 0.5%. Sensitivity analyses for the components' initial capital show PV's initial capital has the greatest impact while WT's initial capital has the least impact on LCOE. When the components' initial capital falls to 80% of its initial value, the LCOE can fall by 3.97% for the PV case, 2.19% for the BS case and 2.07% for the WT case, and when components' initial capital increases to 120% of its initial value, the LCOE can increase by 6.05% for the PV case, 4.77% for the BS case and 2.50% for the WT case. The results indicate that reducing the PV's initial capital produces more obvious economic benefits.

Author Contributions: Conceptualization, Y.Y. and R.L.; data curation, R.L.; formal analysis, Y.Y. and R.L.; funding acquisition, Y.Y.; investigation, Y.Y.; methodology, Y.Y.; project administration, R.L.; software, Y.Y. and R.L.; validation, R.L.; visualization, Y.Y.; writing—original draft, R.L.; writing—review & editing, R.L. All authors have read and agreed to the published version of the manuscript.

Funding: This work was supported by the Natural Science foundation of Jiangsu Province (Grant No. BK20181308), and the Fundamental Research Funds for the Central Universities (Grant No. 2018B45414).

Conflicts of Interest: The authors declare no conflict of interest.

Nomenclature

DOD	BS's allowable depth of discharge
f_{PV}	PV derating factor (%)
G_t	solar incident radiation on the PV (kW/m^2)
G_{STC}	solar radiation under standard test conditions (G_{STC} = 1 kW/m^2)
h	turbine hub altitude (m)
h_{ref}	anemometer altitude (m)
IC	initial capital cost (\$/kW)
i_r	real discount rate (%)
k_{cv}	perturbation factor of load
$O\&M$	maintenance and operation cost (\$/kW)
P_L	electrical load (kW)
P_{PV}	output power of PV (kW)
P_r	rated output power of WT (kW)
P_{WT}	output power of WT (kW)
r	nominal discount rate (%)
Rp	replacement cost (\$/kW)
RV	salvage value(\$/kW)
S_c	a binary variable denoting whether the converter capacity is sufficient
S_p	a binary variable denoting whether the electric power generated is sufficient
SOC_B	SOC BS's state of charge
u	expected inflation rate (%)
v	wind speed at the turbine hub altitude (m/s)
v_{cut-in}	cut-in speed (m/s)
$v_{cut-out}$	cut-out speed (m/s)
v_r	nominal speed (m/s)
v_{ref}	wind speed measured by anemometer (m/s)
α_d	daily variation percent of load
α_t	hourly variation percent of load
η_c	charge efficiency of BS
η_d	discharge efficiency of BS
η_{inv}	converter efficiency

Abbreviation

BS	battery system
CRF	capital recovery factor
DG	diesel system
EMS	energy management strategy
HRES	hybrid renewable energy systems
LCC	life cycle cost
LCOE	levelized cost of electricity
LPSP	loss of power supply probability
WT	wind turbine
PF	Pareto frontier
PS	Pareto set

References

1. Huang, Y.; Li, S.; Ding, P.; Zhang, Y.; Yang, K.; Zhang, W. Optimal Operation for Economic and Exergetic Objectives of a Multiple Energy Carrier System Considering Demand Response Program. *Energies* **2019**, *12*, 3995. [CrossRef]
2. Yang, Y.; Guo, S.; Liu, D.; Li, R.; Chu, Y. Operation optimization strategy for wind-concentrated solar power hybrid power generation system. *Energy Convers. Manag.* **2018**, *160*, 243–250. [CrossRef]

3. Kyritsis, A.; Voglitsis, D.; Papanikolaou, N.; Tselepis, S.; Christodoulou, C.; Gonos, I.; Kalogirou, S.A. Evolution of PV systems in Greece and review of applicable solutions for higher penetration levels. *Renew. Energy* **2017**, *109*, 487–499. [CrossRef]
4. Anoune, K.; Bouya, M.; Astito, A.; Abdellah, A.B. Sizing methods and optimization techniques for PV-wind based hybrid renewable energy system: A review. *Renew. Sustain. Energy Rev.* **2018**, *93*, 652–673. [CrossRef]
5. Zahraee, S.M.; Khalaji Assadi, M.; Saidur, R. Application of Artificial Intelligence Methods for Hybrid Energy System Optimization. *Renew. Sustain. Energy Rev.* **2016**, *66*, 617–630. [CrossRef]
6. Nogueira, C.E.C.; Vidotto, M.L.; Niedzialkoski, R.K.; de Souza, S.N.M.; Chaves, L.I.; Edwiges, T.; dos Santos, D.B.; Werncke, I. Sizing and simulation of a photovoltaic-wind energy system using batteries, applied for a small rural property located in the south of Brazil. *Renew. Sustain. Energy Rev.* **2014**, *29*, 151–157. [CrossRef]
7. Malheiro, A.; Castro, P.M.; Lima, R.M.; Estanqueiro, A. Integrated sizing and scheduling of wind/PV/diesel/battery isolated systems. *Renew. Energy* **2015**, *83*, 646–657. [CrossRef]
8. Li, J.L.; Guo, B.Q.; Niu, M.; Xiu, X.Q.; Tian, L.T. Optimal Configuration Strategy of Energy Storage Capacity in Wind/PV/Storage Hybrid System. *Trans. China Electrotech. Soc.* **2018**, *33*, 1189–1196.
9. Smaoui, M.; Abdelkafi, A.; Krichen, L. Optimal sizing of stand-alone photovoltaic/wind/hydrogen hybrid system supplying a desalination unit. *Sol. Energy* **2015**, *120*, 263–276. [CrossRef]
10. Bhuiyan, F.A.; Yazdani, A.; Primak, S.L. Optimal sizing approach for islanded microgrids. *IET Renew. Power Gener.* **2015**, *9*, 166–175. [CrossRef]
11. Al-falahi, M.D.A.; Jayasinghe, S.D.G.; Enshaei, H. A review on recent size optimization methodologies for standalone solar and wind hybrid renewable energy system. *Energy Convers. Manag.* **2017**, *143*, 252–274. [CrossRef]
12. HOMER Pro Version 3.7 User Manual. Available online: https://www.homerenergy.com (accessed on 15 December 2019).
13. Lambert, T.; Gilman, P.; Lilienthal, P. Micropower System Modeling with HOMER. 2006. Available online: http://homerenergy.com/documents/MicropowerSystemModelingWithHOMER.pdf (accessed on 15 December 2019).
14. Shahzad, M.K.; Zahid, A.; ur Rashid, T.; Rehan, M.A.; Ali, M.; Ahmad, M. Techno-economic feasibility analysis of a solar-biomass off grid system for the electrification of remote rural areas in Pakistan using HOMER software. *Renew. Energy* **2017**, *106*, 264–273. [CrossRef]
15. Halabi, L.M.; Mekhilef, S.; Olatomiwa, L.; Hazelton, J. Performance analysis of hybrid PV/diesel/battery system using HOMER: A case study Sabah, Malaysia. *Energy Convers. Manag.* **2017**, *144*, 322–339. [CrossRef]
16. Hossain, M.; Mekhilef, S.; Olatomiwa, L. Performance evaluation of a stand-alone PV-wind-diesel-battery hybrid system feasible for a large resort center in South China Sea, Malaysia. *Sustain. Cities Soc.* **2017**, *28*, 358–366. [CrossRef]
17. Li, C.; Zhou, D.; Wang, H.; Lu, Y.; Li, D. Techno-economic performance study of stand-alone wind/diesel/battery hybrid system with different battery technologies in the cold region of China. *Energy* **2020**, *192*, 116702. [CrossRef]
18. Park, E.; Kwon, S.J. Towards a Sustainable Island: Independent optimal renewable power generation systems at Gadeokdo Island in South Korea. *Sustain. Cities Soc.* **2016**, *23*, 114–118. [CrossRef]
19. Rajbongshi, R.; Borgohain, D.; Mahapatra, S. Optimization of PV-biomass-diesel and grid base hybrid energy systems for rural electrification by using HOMER. *Energy* **2017**, *126*, 461–474. [CrossRef]
20. Singh, A.; Baredar, P.; Gupta, B. Techno-economic feasibility analysis of hydrogen fuel cell and solar photovoltaic hybrid renewable energy system for academic research building. *Energy Convers. Manag.* **2017**, *145*, 398–414. [CrossRef]
21. Zahboune, H.; Zouggar, S.; Krajacic, G.; Varbanov, P.S.; Elhafyani, M.; Ziani, E. Optimal hybrid renewable energy design in autonomous system using Modified Electric System Cascade Analysis and Homer software. *Energy Convers. Manag.* **2016**, *126*, 909–922. [CrossRef]
22. Sinha, S.; Chandel, S.S. Review of recent trends in optimization techniques for solar photovoltaic–wind based hybrid energy systems. *Renew. Sustain. Energy Rev.* **2015**, *50*, 755–769. [CrossRef]
23. Singh, S.; Kaushik, S.C. Optimal sizing of grid integrated hybrid PV-biomass energy system using artificial bee colony algorithm. *IET Renew. Power Gener.* **2016**, *10*, 642–650. [CrossRef]

24. Shivaie, M.; Mokhayeri, M.; Kiani-Moghaddam, M.; Ashouri-Zadeh, A. A reliability-constrained cost-effective model for optimal sizing of an autonomous hybrid solar/wind/diesel/battery energy system by a modified discrete bat search algorithm. *Sol. Energy* **2019**, *189*, 344–356. [CrossRef]
25. Bukar, A.L.; Tan, C.W.; Lau, K.Y. Optimal sizing of an autonomous photovoltaic/wind/battery/diesel generator microgrid using grasshopper optimization algorithm. *Sol. Energy* **2019**, *188*, 685–696. [CrossRef]
26. Ramli, M.A.M.; Bouchekara, H.R.E.H.; Alghamdi, A.S. Optimal sizing of PV/wind/diesel hybrid microgrid system using multi-objective self-adaptive differential evolution algorithm. *Renew. Energy* **2018**, *121*, 400–411. [CrossRef]
27. Kamjoo, A.; Maheri, A.; Dizqah, A.M.; Putrus, G.A. Multi-objective design under uncertainties of hybrid renewable energy system using NSGA-II and chance constrained programming. *Int. J. Electr. Power Energy Syst.* **2016**, *74*, 187–194. [CrossRef]
28. Nasiraghdam, H.; Jadid, S. Optimal hybrid PV/WT/FC sizing and distribution system reconfiguration using multi-objective artificial bee colony (MOABC) algorithm. *Sol. Energy* **2012**, *86*, 3057–3071. [CrossRef]
29. Mazzeo, D.; Baglivo, C.; Matera, N.; Congedo, P.M.; Oliveti, G. A novel energy-economic-environmental multi-criteria decision-making in the optimization of a hybrid renewable system. *Sustain. Cities Soc.* **2020**, *52*, 101780. [CrossRef]
30. Qingfu, Z.; Hui, L. MOEA/D: A Multiobjective Evolutionary Algorithm Based on Decomposition. *IEEE Trans. Evol. Comput.* **2007**, *11*, 712–731. [CrossRef]
31. Xinye, C.; Yexing, L.; Zhun, F.; Qingfu, Z. An External Archive Guided Multiobjective Evolutionary Algorithm Based on Decomposition for Combinatorial Optimization. *IEEE Trans. Evol. Comput.* **2015**, *19*, 508–523. [CrossRef]
32. Amrollahi, M.H.; Bathaee, S.M.T. Techno-economic optimization of hybrid photovoltaic/wind generation together with energy storage system in a stand-alone micro-grid subjected to demand response. *Appl. Energy* **2017**, *202*, 66–77. [CrossRef]
33. Zhang, J.; Sanderson, A.C. JADE: Adaptive differential evolution with optional external archive. *IEEE Trans. Evol. Comput.* **2009**, *13*, 945–958. [CrossRef]
34. Tian, Y.; Cheng, R.; Zhang, X.; Jin, Y. PlatEMO: A MATLAB Platform for Evolutionary Multi-Objective Optimization [Educational Forum]. *IEEE Comput. Intell. Mag.* **2017**, *12*, 73–87. [CrossRef]
35. Zitzler, E.; Deb, K.; Thiele, L. Comparison of multiobjective evolutionary algorithms: Empirical results. *Evol. Comput.* **2000**, *8*, 173–195. [CrossRef] [PubMed]
36. Coello, C.A.; Cortés, N.C. Solving multiobjective optimization problems using an artificial immune system. *Genet. Program. Evolvable Mach.* **2005**, *6*, 163–190. [CrossRef]
37. 2019 ATB. Available online: https://atb.nrel.gov/electricity/2019/ (accessed on 12 March 2020).

© 2020 by the authors. Licensee MDPI, Basel, Switzerland. This article is an open access article distributed under the terms and conditions of the Creative Commons Attribution (CC BY) license (http://creativecommons.org/licenses/by/4.0/).